


Cite this: *RSC Adv.*, 2022, 12, 13487

First-row transition metal doped germanium clusters Ge_{16}M : some remarkable superhalogens†

Huu Tho Nguyen,^a Ngo Tuan Cuong,^b Ngo Thi Lan,^{cd} Nguyen Thanh Tung,^c Minh Tho Nguyen^{de} and Nguyen Minh Tam^{dfg}

A theoretical study of geometric and electronic structures, stability and magnetic properties of both neutral and anionic $\text{Ge}_{16}\text{M}^{0/-}$ clusters with M being a first-row 3d transition metal atom, is performed using quantum chemical approaches. Both the isoelectronic $\text{Ge}_{16}\text{Sc}^-$ anion and neutral Ge_{16}Ti that have a perfect Frank–Kasper tetrahedral T_d shape and an electron shell filled with 68 valence electrons, emerge as magic clusters with an enhanced thermodynamic stability. The latter can be rationalized by the simple Jellium model. Geometric distortions from the Frank–Kasper tetrahedron of Ge_{16}M having more or less than 68 valence electrons can be understood by a Jahn–Teller effect. Remarkably, DFT calculations reveal that both neutral Ge_{16}Sc and Ge_{16}Cu can be considered as superhalogens as their electron affinities (≥ 3.6 eV) exceed the value of the halogen atoms and even that of icosahedral Al_{13} . A detailed view of the magnetic behavior of $\text{Ge}_{16}\text{M}^{0/-}$ clusters shows that the magnetic moments of the atomic metals remain large even when they are quenched upon doping. When M goes from Sc to Zn, the total spin magnetic moment of $\text{Ge}_{16}\text{M}^{0/-}$ increases steadily and reaches the maximum value of $3 \mu_B$ with M = Mn before decreasing towards the end of the first-row 3d block metals. Furthermore, the IR spectra of some tetrahedral Ge_{16}M are also predicted.

Received 21st November 2021
Accepted 26th April 2022

DOI: 10.1039/d1ra08527a

rsc.li/rsc-advances

1. Introduction

Along with silicon, germanium is one of the most important microelectronic materials. The last several decades have witnessed a continuing interest in the clusters of this semiconductor element since their bulk materials can no longer satisfy the current needs of the miniaturization of electronic devices.^{1–11} Both silicon and germanium do not favor sp^2 -hybridization such as carbon whose small clusters tend to form linear or planar cyclic structures, but rather prefer 3D species arising from a tetrahedral sp^3 hybridization. Consequently, pure germanium clusters with high symmetry are often

unstable in the form of empty caged structures. Since the first observation of the far more abundant Si_{15}M and Si_{16}M that was reported in 1987 from the laser photoionization time of flight mass spectra,¹² subsequent investigations using *ab initio* calculations on the geometrical and electronic structures of the Si_{15} and Si_{16} clusters doped with several transition metals such as Cr, Mo, and W have been performed.¹³ These studies showed that the transition metal dopant is often located inside a polyhedral cage forming the Si_{15}M and Si_{16}M clusters that have high thermodynamic stability and low magnetic moments as compared the M metal dopants. In a recent review article, Kumar *et al.*¹⁴ analyzed in detail the electronic and geometrical structures of the Si_{15} and Si_{16} clusters doped with several transition metals and showed that the transition metal atom is always endohedrally doped within the silicon cage. This thus demonstrates that introduction of hetero-atoms as dopants into hollow cages can supply us with a valuable pathway to stabilize endohedral cage-like clusters as well as to adjust their many novel physico-chemical properties. Motivated by such a fundamental feature, along with several studies performed on doped silicon clusters, a large number of both experimental and theoretical investigations on germanium clusters doped by various chemical elements have been carried out.^{15–39}

Transition metal atoms that have unpaired valence electrons in their *nd* electronic configurations, are inherently magnetic elements. They have been considered as interesting dopants in clusters since interactions between these impurities and the host

^aFaculty of Natural Sciences Education, Sai Gon University, 273 An Duong Vuong Street, Ho Chi Minh City, Vietnam

^bCenter for Computational Science, Faculty of Chemistry, Hanoi National University of Education, Hanoi, Vietnam

^cInstitute of Materials Science and Graduate University of Science and Technology, Vietnam Academy of Science and Technology, 18 Hoang Quoc Viet, Hanoi, Vietnam

^dInstitute of Science and Technology, TNU-University of Sciences, Tan Thinh Ward, Thai Nguyen City, Vietnam

^eInstitute for Computational Science and Technology (ICST), Quang Trung Software City, Ho Chi Minh City, Vietnam

^fLaboratory of Theoretical and Computational Biophysics, Advanced Institute of Materials Science, Ton Duc Thang University, Ho Chi Minh City, Vietnam. E-mail: nguyennminhtam@tdtu.edu.vn

^gFaculty of Pharmacy, Ton Duc Thang University, Ho Chi Minh City, Vietnam

† Electronic supplementary information (ESI) available. See <https://doi.org/10.1039/d1ra08527a>


are expected to alter both electronic and geometrical structures and thereby to generate the doped clusters possessing some novel physico-chemical properties. Moreover, as stated above, due to their high coordination number, transition metals can endohedrally be doped and stabilize the caged structures and simultaneously tailor magnetic properties of host clusters. Indeed, previous studies of singly transition metal doped germanium clusters showed that starting from the size $n = 9$, the Ge unit absorbs the Ni and Ru dopant endohedrally in giving rise to the most stable isomers of Ge_nNi and Ge_nRu .^{22,24} The metal atom is encapsulated inside a germanium cage at $n = 10$ when the dopant is Ti, V, and Cu,^{20,25,29} and the critical size for the heavy metal W atom being completely enclosed into a caged germanium framework in the Ge_nW clusters turns out to be at $n = 12$.³³ A theoretical investigation³⁴ on divalent-metal atom doped silicon, germanium and tin clusters X_nM ($\text{X} = \text{Si}, \text{Ge}, \text{Sn}; n = 8-12$ and 14) demonstrated that the 12- and 14-atom clusters can be transformed into magic clusters upon doping. Particularly, the manganese-doped X_{12}Mn was found to be an icosahedral superatom with a high magnetic moment of $5 \mu_B$.³⁴ In an examination of doubly iron-doped germanium clusters, Liang and co-workers also indicated that both neutral and cationic states of $\text{Ge}_n\text{Fe}_2^{0/-}$ adopt polyhedral cage-like shapes with one Fe atom located inside the cage with $9 \leq n \leq 12$.²⁶ Soon after the theoretical prediction of metal-encapsulated silicon cages,⁴⁰ Kumar and Kawazoe performed a series of calculations to explore the possible germanium cages stabilized by metal doping. Analogous to M@Si_n clusters, they explored M@Ge_n ($n = 14-16$ and $\text{M} = \text{Ti}, \text{Zr}, \text{Hf}, \text{Fe}, \text{Ru}, \text{Os}$) clusters with various possible cage configurations such as the Frank-Kasper (FK) polyhedron, capped decahedron, fullerene-like cage and cubic cage.⁴¹⁻⁴⁴ Remarkably, the Ge_{16}M sizes have been one of the most attractive germanium clusters that have been reported so far. A quantum chemical study of Kumar *et al.*⁴¹ revealed that the very stable ground states of Ge_{16}M clusters, with M being elements of Group IVb including Ti, Zr, and Hf, are FK tetrahedra characterized by large HOMO-LUMO energy gaps. Surprisingly, the energy gap for Ge_{16}Zr is even larger than the value for the lowest-energy isomer of FK Si_{16}Zr discovered before.⁴⁰ Most recently, Du and co-workers carried out an investigation on the interaction in dimers of well-known endohedrally doped clusters, including several X_{16}M clusters with X being the tetravalent elements, and found that Ge_{16}Ti cage clusters emerge as suitable building blocks to assemble generating solids and nanostructures with enhanced stabilities and diverse physical properties.⁴⁵

To date, many transition metal-silicon and transition metal-germanium clusters have been examined, and the understanding on the cage-like silicon and germanium structures stabilized by doping of some transition metals has well been established on the basis of the concept of filling the electron shells for superatoms within a spherical potential model, and also of various electron counting rules including the Wade-Mingos rules, systems with 18 and 32 electrons.¹⁴ However, to the best of our knowledge, until recently only one study on the trimeric Ge_2M including all 3d transition metals M was reported.⁴⁶ Therefore, systematic theoretical studies on a certain series of transition metal-germanium clusters are still necessary

in order to understand more deeply the relationship between structures and electronic properties of the transition metal doped Ge cluster, especially the Ge_{16} ones bearing the characteristic Frank-Kasper geometry. In this context, we set out to perform a systematic theoretical investigation on the geometries, stability, and magnetic properties of the germanium clusters doped by one atom belonging to the 3d row transition metals in both neutral and anionic states $\text{Ge}_{16}\text{M}^{0/-}$, with M going from Sc to Zn. Using density functional theory (DFT) calculations, we thoroughly determine the geometries of the lowest-lying equilibrium structures and thereby explore their structural evolution, as well as assign their electronic configurations, energetic parameters and magnetic properties. In particular, some systems behaving as strong superhalogens are discovered.

2. Computational methods

On the basis of a reliability test that has been obtained from a previous study on germanium-based clusters,²¹ we select the hybrid B3PW91 functional in conjunction with the 6-311+G(d) basis sets as implemented in Gaussian 09 package⁴⁷ for all electronic structure calculations carried out in this work. The unrestricted formalism is used for species with an open electronic shell. The search for local energy minima is conducted using the two approaches. First, plausible structures of Ge_{16}M clusters are generated using a stochastic algorithm,⁴⁸ which was improved based on the random kick procedure reported by Saunders.⁴⁹ By another way, initial structures of each Ge_{16}M are manually constructed by adding the M atom at all possible positions on the surfaces of the reported low-lying isomers of Ge_{16} .^{10,11} The initial guess structures are then geometrically optimized using the hybrid B3PW91 functional in conjugation with the small LANL2DZ basis set. Several local minima obtained by different approaches turn out to be identical. The local energy minima having relative energies of <5 eV with respect to the lowest-lying isomer are then reoptimized at different spin states using the same B3PW91 functional but with the larger 6-311+G(d) basis set. Harmonic vibrational frequencies and zero-point energy (ZPE) corrections of the Ge_{16}M clusters are subsequently calculated at the same level. Unless otherwise stated, relative energies quoted hereafter are determined from B3PW91/6-311+G(d) + ZPE computations.

Furthermore, the natural bond orbital (NBO) analyses are performed by using the NBO 3.0 program implemented in the Gaussian package to examine the electronic configuration and thereby rationalize the magnetic and chemical bonding properties of the clusters considered. Based on the NBO analyses, the magnetic moments including the total (TMMs) and local (LMMs) values are defined as the difference between the numbers of spin-up and spin-down electrons occupying the molecular/atomic orbitals of the cluster/atom.

3. Results and discussion

3.1. Geometrical structures

Shapes of the optimized equilibrium structures of both neutral and anionic series of Ge_{16}M clusters, their spin states, and DFT



relative energies are shown in Fig. 1 and 2. Because of the large number of isomers located on the potential energy surface of each cluster, only some low lying isomers whose relative energies are close to the corresponding ground state structure are presented for each dopant M.

As for a convention, a **X.M.Y** label is used to denote the isomers considered, in which **X = n** and **a** stand for a neutral and anionic state, respectively, **M = Sc, Ti, V, Cr, Mn, Fe, Co, Ni, Cu, and Zn**, and **Y = A, B, C...** refers to the different isomers with increasing relative energy. Thus, **X.M.A** invariably refers to the lowest-energy isomer of the **X.M** series.

The main characteristics of the geometrical features can briefly be summarized as follows:

For **M = Sc, Ti and V**, our calculated results are in good agreement with the previous studies.^{36,41} The most stable Ge_{16}M in both neutral and anionic states consistently prefer a FK structure in which the dopant atom is endohedrally located at the central position of the FK Ge_{16} cage. Remarkably, the lowest-lying isomers of both isoelectronic $\text{Ge}_{16}\text{Sc}^-$ anion and Ge_{16}Ti neutral are much more stable than the next isomers with large relative energy gaps of 0.84 and 0.95 eV, respectively. The most stable Ge_{16}V in both neutral and anionic states still retain the FK form, but their relative energy gaps decrease to <0.5 eV. Besides, the low-lying isomers of Ge_{16}V^- anion are found to exist in the triplet state.

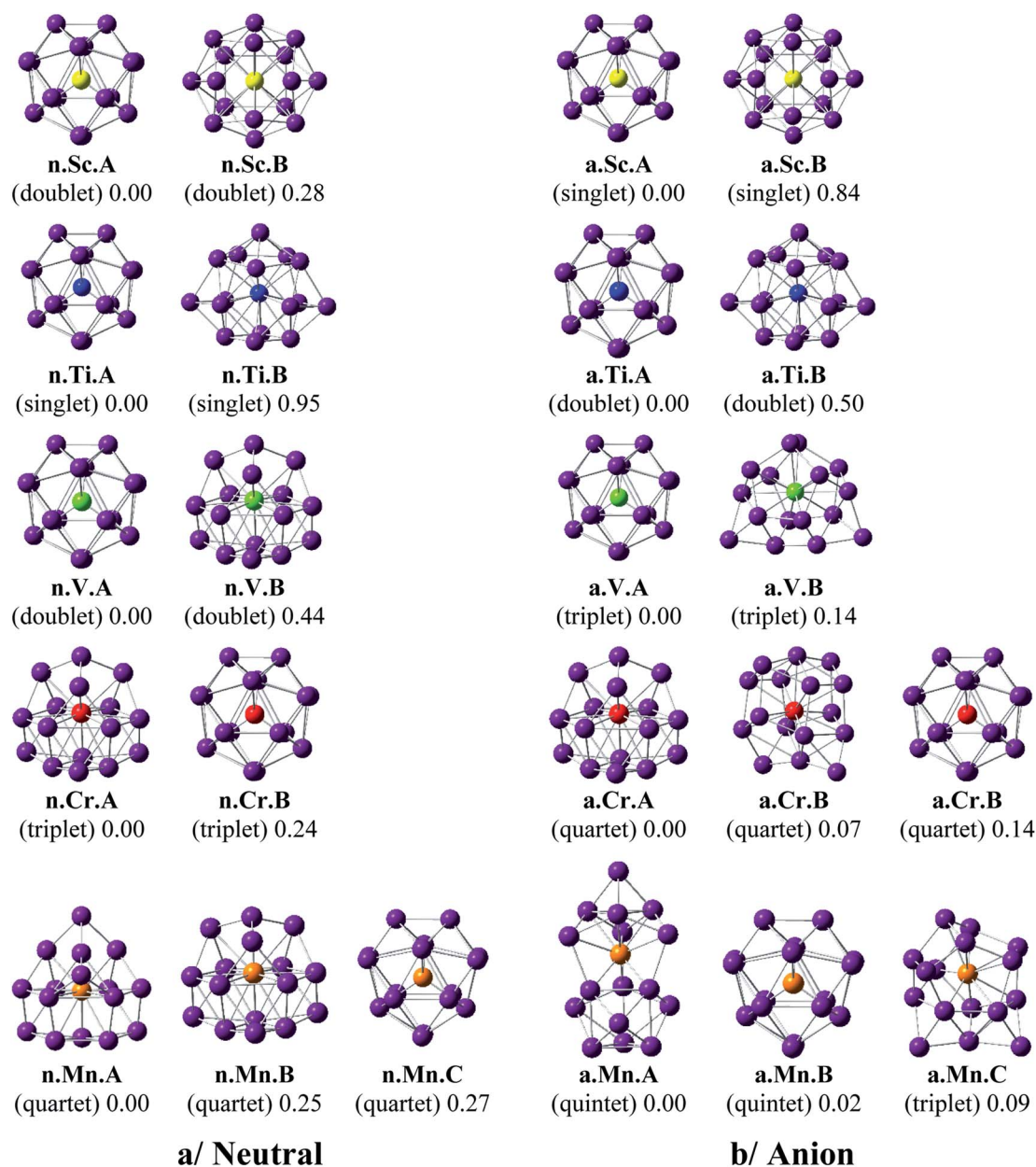


Fig. 1 Geometry, relative energy, and spin state (in the bracket) of the most stable isomers $\text{Ge}_{16}\text{M}^{0/-}$, with **M = Sc, Ti, V, Cr, and Mn** using (U) B3PW91/6-311+G(d) optimizations.



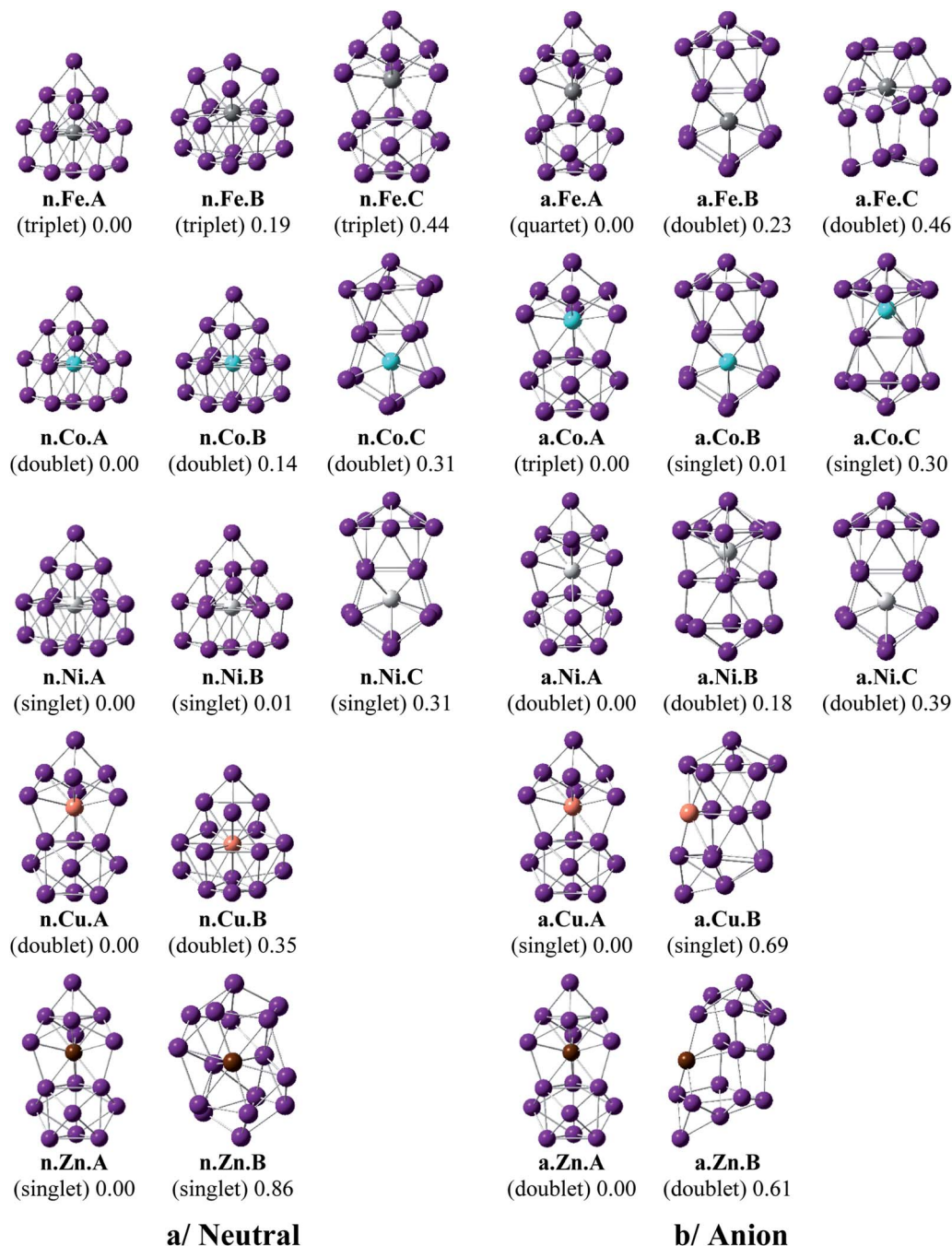


Fig. 2 Geometry, relative energy, and spin state (in the bracket) of the most stable isomers $\text{Ge}_{16}\text{M}^{0/-}$, with $\text{M} = \text{Fe}, \text{Co}, \text{Ni}, \text{Cu}$, and Zn using (U) B3PW91/6-311+G(d) optimizations.

For Ge_{16}Cr , the FK is no longer the most stable form, as they are 0.24 and 0.14 eV higher in energy than the neutral and anion, respectively, of another endohedral structure in which the Cr atom is encapsulated in a C_{3v} cage. Ge_{16}Cr also favors high spin multiplicity, corresponding to the triplet and quartet states for the neutral and anion, respectively.

The three lowest lying isomers of the neutral Ge_{16}Mn prefer endohedrally doped structures and are stable in a quartet state. **n.Mn.A** becomes 0.25 eV more stable than the other cage **n.Mn.B**. In the anionic state, however, a competition in energy

among three most stable isomers emerges with relative energy gaps of <0.1 eV. Particularly, the **a.Mn.A**, constructed from fusion of two Ge_{10} in which the endohedral Ge atom, or the Ge atom at the vertex of the lower Ge_{10} block, is substituted by the Mn atom,⁴⁸ and the FK **a.Mn.B**, are energetically degenerate within a small energy difference of only 0.02 eV, and both of them have a magnetic moment of $4 \mu_{\text{B}}$, arising from a quintet spin state. Remarkably, the geometry of **a.Mn.A** is also retained as the most stable one for all remaining Ge_{16}M^- anions, with M being Fe, Co, Ni, Cu and Zn, despite a competition in energy in



$\text{Ge}_{16}\text{Co}^-$ where the triplet state **a.Co.A** is only 0.01 eV lower in energy than the singlet **a.Co.B**. Accordingly, both Co derivatives **a.Co.A** and **a.Co.B** are energetically degenerate.

The shapes of the low lying isomers of the neutral Ge_{16}Fe , Ge_{16}Co , and Ge_{16}Ni are similar to that of the Ge_{16}Mn . However, optimization calculations indicate that the two endohedral isomers **n.Ni.A** and **n.Ni.B** of Ge_{16}Ni are again practically degenerate with a negligible energy gap of 0.01 eV. Finally, the lowest-lying isomers of Ge_{16}Cu and Ge_{16}Zn exhibit the same shape in both neutral and anionic states.

3.2. Stabilities

In order to probe the inherent thermodynamic stability of the Ge_{16}M clusters considered, their average binding energies (E_b) are examined and compared to those of the relevant pure germanium clusters Ge_{17} in both neutral and anionic states. The E_b values of the Ge_{16}M clusters can conventionally be defined in eqn (1) and (2):

$$E_b(\text{Ge}_{16}\text{M}) = [16E(\text{Ge}) + E(\text{M}) - E(\text{Ge}_{16}\text{M})]/17 \quad (1)$$

$$E_b(\text{Ge}_{16}\text{M}^-) = [15E(\text{Ge}) + E(\text{Ge}^-) + E(\text{M}) - E(\text{Ge}_{16}\text{M}^-)]/17 \quad (2)$$

where $E(\text{Ge})$, $E(\text{Ge}^-)$, and $E(\text{M})$, are the total energies of the Ge-atom, the anion Ge^- , and the M-atom, respectively. $E(\text{Ge}_{16}\text{M})$ and $E(\text{Ge}_{16}\text{M}^-)$ are the total energies of the neutral and anionic of Ge_{16}M , respectively.

Similarly, for the neutral Ge_{17} and anionic Ge_{17}^- , the E_b can be defined by eqn (3) and (4), respectively, as follows:

$$E_b(\text{Ge}_{17}) = [17E(\text{Ge}) - E(\text{Ge}_{17})]/17 \quad (3)$$

$$E_b(\text{Ge}_{17}^-) = [16E(\text{Ge}) + E(\text{Ge}^-) - E(\text{Ge}_{17}^-)]/17 \quad (4)$$

where $E(\text{Ge}_{17})$ and where $E(\text{Ge}_{17}^-)$ are the total energies of the pure neutral and anionic Ge_{17} , respectively, that were reported in the previous studies.^{10,11} All these energy values are obtained from B3PW91/6-311+G(d) + ZPE calculations and the plots of E_b depicted in Fig. 3a illustrate their evolution. The trends of E_b values in both neutral and anionic Ge_{16}M are quite similar to each other. In comparison to the E_b value of Ge_{17} , the E_b values of Ge_{16}M are higher when the M dopant goes from Sc to V, then decrease to lower values with M being Cr and Mn. As M goes from Fe to Ni, the E_b values of $\text{Ge}_{16}\text{M}^{0/-}$ return to be higher than that of $\text{Ge}_{17}^{0/-}$. For M = Cu, the E_b value of the neutral Ge_{16}Cu is approximately equal to that of Ge_{17} whereas that of the anionic $\text{Ge}_{16}\text{Cu}^-$ becomes lower than the corresponding value of Ge_{17}^- . Finally, Ge_{16}Zn takes the lowest E_b values in both neutral and anionic states. These calculated results prove that a doping of the first-row transition metal M, except for Cr, Mn, Cu and Zn, into Ge_{16} enhances the cluster stability as compared to the pure germanium clusters Ge_{17} in both neutral and anionic states. Remarkably, the neutral Ge_{16}Ti and anionic $\text{Ge}_{16}\text{Sc}^-$, which possesses each 68 valence electrons, reveal the highest E_b values as compared to the remaining Ge_{16}M counterparts.

To reinforce the above findings, we further examine the embedding energy (EE) of the clusters considered. Embedding

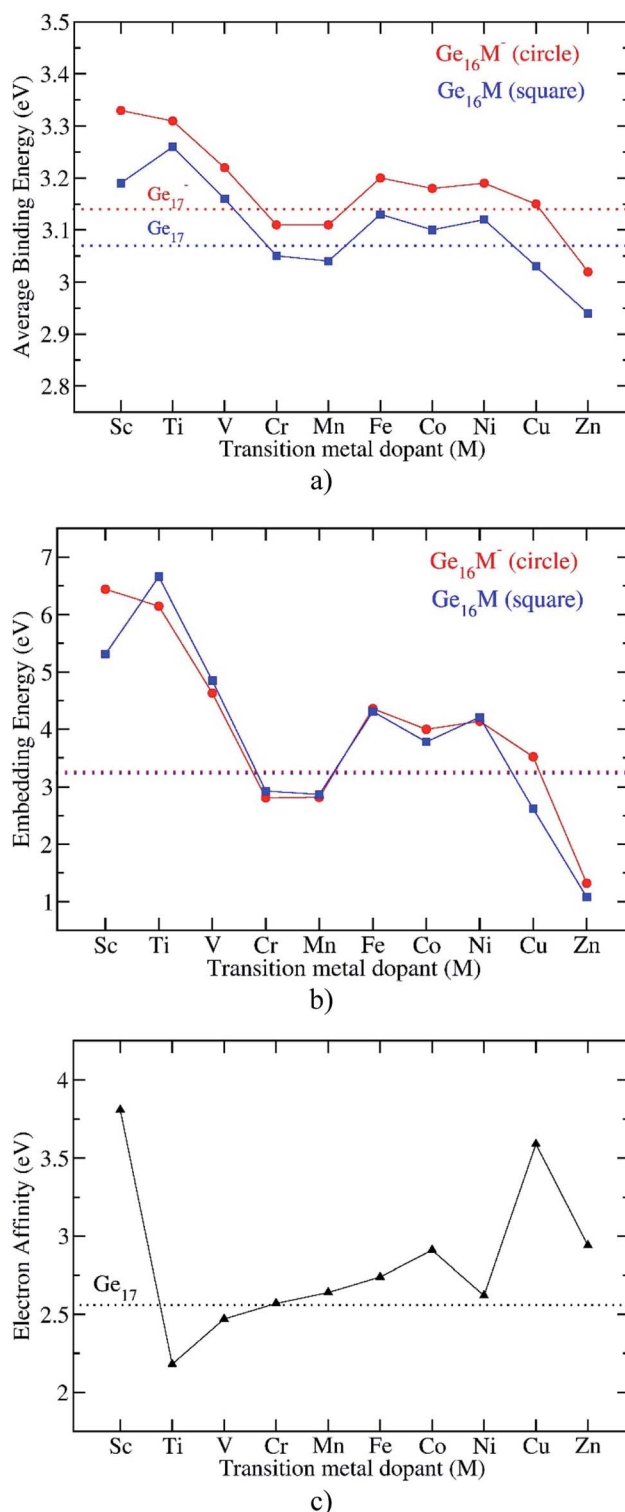


Fig. 3 Evolution of the average binding energy, embedding energy, and electron affinity of the Ge_{16}M clusters considered. Values are obtained from (U)B3PW91/6-311+G(d) + ZPE computations.

energy is defined as the energy gained in incorporating a M-dopant into the Ge_{16} hosts and defined by eqn (5):

$$EE(\text{Ge}_{16}\text{M}^{0/-}) = E(\text{Ge}_{16}^{0/-}) + E(\text{M}) - E(\text{Ge}_{16}\text{M}^{0/-}) \quad (5)$$



where $E(\text{Ge}_{16}^{0/-})$ are the total DFT energies of the neutral and anionic Ge_{16} clusters, respectively. These total energies are calculated for the ground states of the pure clusters $\text{Ge}_{16}^{0/-}$ which were previously reported.^{10,11} Fig. 3b indicates that both Ge_{16}Ti and $\text{Ge}_{16}\text{Sc}^-$ are really characterized by the highest EE values for the neutral Ge_{16}M and anionic Ge_{16}M^- clusters, respectively. These predictions are in good agreement with the E_b values mentioned above, and it can thus be concluded from these observations that an enhanced thermodynamic stability is established for both isoelectronic Ge_{16}Ti and $\text{Ge}_{16}\text{Sc}^-$ species.

The E_b values of all anionic Ge_{16}M^- and pure Ge_{17}^- clusters are obviously higher than those of the neutral counterparts, as shown in Fig. 3a. An examination of the computed adiabatic electron affinities (EA) of neutral Ge_{16}M , in comparison to that of Ge_{17} , can thus give us a better insight into this feature. As shown in Fig. 3c, except for Ti and V, the first-row transition metal doped germanium clusters Ge_{16}M have the larger EA values than that of Ge_{17} . When the M-dopant varies from Sc to Zn, the EA of Ge_{16}M takes the largest value of 3.8 eV at Ge_{16}Sc , then decrease sharply and reaches the lowest value of 2.2 eV at the next member Ge_{16}Ti . Then, the EA value gradually increases as M-dopant goes from Ti to Co, then slightly decreases at Ge_{16}Ni before strongly increases at the coinage metal Ge_{16}Cu and finally decreases again at Ge_{16}Zn .

The large EA of Ge_{16}Sc can be interpreted in the same way as that applied to the neutral Al_{13} , which is well-known for its very large electron affinity exceeding that of halogen atoms and has thus been named as a superhalogen.⁵⁰ Similarly, the neutral Ge_{16}Sc , as formed from the detachment of one electron from the closed-shell structure of the anion $\text{Ge}_{16}\text{Sc}^-$ possessing an enhanced thermochemical stability, also has a very large electron affinity. As stated above, calculations reveal that the EA of Ge_{16}Sc amounts to 3.8 eV, which is even larger than that of 3.6 eV of Al_{13} .⁵¹ In contrast to Ge_{16}Sc , the following neutral member Ge_{16}Ti , which is stabilized by a closed shell filled by 68 valence electrons in a singlet state, exhibits the smallest EA value due to the low stability of the corresponding anion. In this context, Ge_{16}Sc can be considered as a superhalogen.

The enhanced stability of both isoelectronic Ge_{16}Ti and $\text{Ge}_{16}\text{Sc}^-$ FK structures can be rationalized by examining their MO pictures under the viewpoint of the electronic shells in a Jellium model (JM),⁵² which is successfully applied to clarify the stability of various structural motifs of atomic clusters in previous studies, particularly those based on Group IVa atoms.^{48,53,54} According to this simple model, the valence electrons are freely movable in a simple mean-field potential constructed by the nuclei of atoms; the valence electrons fill the orbitals following the pattern of atomic orbitals (AO) as $[1\text{S}^2 1\text{P}^6 1\text{D}^{10} 2\text{S}^2 1\text{F}^{14} 2\text{P}^6 1\text{G}^{18} 2\text{D}^{10} \dots]$ corresponding to the numbers of electrons of 2, 8, 18, 20, 34, 40, 58 and 68, *etc.*, that emerge as the magic numbers consistent with a complete filling of the successive electronic shells. As a consequence, a cluster that possesses a valence electron number belonging to this magic number series is able to attain an enhanced thermodynamic stability.

Both Ge_{16}Ti and $\text{Ge}_{16}\text{Sc}^-$ FK's are characterized by a closed electronic shell configuration with the magic number of 68 valence electrons. The shapes of the relevant MOs and their

energy levels, as illustrated in Fig. 4, reveal the great similarity between their densities of states (DOS) and thus prove that they have similar electronic structure as well as the thermochemical stability. The 68 valence electrons of each cluster are distributed in the following orbital configuration:

$$[(1\text{A}_1)^2 (1\text{T}_2)^6 (1\text{E})^4 (2\text{T}_2)^6 (2\text{A}_1)^2 (3\text{T}_2)^6 (1\text{T}_1)^6 (3\text{A}_1)^2 (4\text{A}_1)^2 (4\text{T}_2)^6 (2\text{T}_1)^6 (5\text{T}_2)^6 (2\text{E})^4 (3\text{E})^4 (6\text{T}_2)^6].$$

This corresponds to a sequence of electronic shell model as:

$$[1\text{S}^2 1\text{P}^6 1\text{D}^{10} 1\text{F}^{14} 2\text{S}^2 1\text{G}^2 2\text{P}^6 1\text{G}^{16} 2\text{D}^{10}]$$

For both clusters, the lowest-lying MOs include an s-type valence orbital of the 1S and three p-type orbitals of the 1P

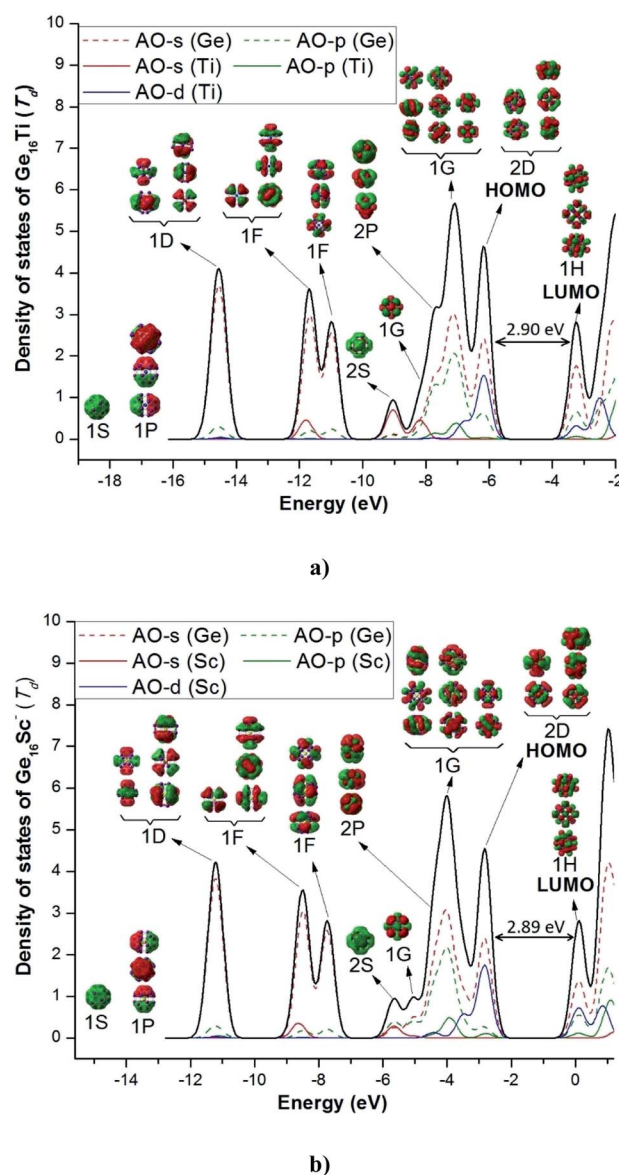


Fig. 4 Total (DOS) and partial (pDOS) densities of state of (a) Ge_{16}Ti and (b) $\text{Ge}_{16}\text{Sc}^-$. Shapes of orbitals of clusters are obtained from B3PW91/6-311+G(d) calculations.



subshells. The MOs of both 1D and 1F subshells are mainly composed of s-AO of Ge and the remaining AOs of both germanium and the transition metal dopant with much smaller contributions. For the neutral Ge_{16}Ti , the MO of 2S subshell are principally formed by the s-AO(Ti), whereas the MO of 2S of anion $\text{Ge}_{16}\text{Sc}^-$ are constructed by interaction between s-AO(Sc) and p-AOs(Ge). The MOs of 2P and 1G subshells are constructed by a combination of both s- and p-AOs of Ge-atoms. Finally, the 2D subshell is composed of both s- and p-AO of Ge and d-AO of the metal impurity. In general, the electronic configuration of the both neutral Ge_{16}Ti and anion $\text{Ge}_{16}\text{Sc}^-$ basically satisfies the electronic shell model of $[1\text{S}^2 1\text{P}^6 1\text{D}^{10} 1\text{F}^{14} 2\text{S}^2 1\text{G}^2 2\text{P}^6 1\text{G}^{16} 2\text{D}^{10}]$ and makes them the enhanced stability species with a magic number of 68 valence electrons.

Remarkably, in addition to the finding of Ge_{16}Sc superhalogen, calculations reveal that the ground state of the anion $\text{Ge}_{16}\text{Cu}^-$ also has a closed electronic shell and high stability as compared to its neutral form, and being much more stable than the second isomer with a large relative energy gap of 0.69 eV. This is caused by the fact that the neutral Ge_{16}Cu has a large electron affinity of 3.6 eV, again approximate to those of the chlorine atom and Al_{13} mentioned above. Accordingly, Ge_{16}Cu can also be considered as a superhalogen. The large EA of Ge_{16}Cu can be interpreted based on MO approaches. Of the Ge_{16}M clusters in both neutral and anionic forms, the electronic structure of the anion $\text{Ge}_{16}\text{Cu}^-$ can be considered as a closed-shell by 68 electrons in the pool of valence electrons of the whole cluster such as in the case of $\text{Ge}_{16}\text{Sc}^-$ and Ge_{16}Ti even though it possesses a non-spherical like geometry. This could be rationalized by considering the following fact. Each Ge delocalizes four electrons whereas the Cu dopant delocalizes three of its eleven $4\text{s}^1 3\text{d}^{10}$ valence electrons including one 4s and two 3d into the pool, and while the added electrons are also delocalized in the shell of the entire cluster, the eight remaining 3d electrons are localized in four 3d orbitals of the central Cu. The reason for such a behaviour of the Cu atom in the $\text{Ge}_{16}\text{Cu}^-$ anion is that it is located at the trigonal-prismatic hole formed by six nearest Ge atoms. Following the ligand field effects induced by the trigonal-prismatic coordination within a C_{3v} point group of the whole $\text{Ge}_{16}\text{Cu}^-$ cluster, the five degenerate 3d AOs of the Cu atoms split into three groups of $E(\text{d}_{xz}, \text{d}_{yz})$, $E(\text{d}_{x^2-y^2}, \text{d}_{xy})$ and $A(\text{d}_{z^2})$ irreducible representations. While the two former groups have lower energies, the latter possessing higher energy matches the energies of the valence AOs of the Ge neighboring atoms, and thereby combine well with them to form shell MOs of the resulting cluster. Based on shapes and relative energies of the MOs, we can now assign the electronic energy levels of the anion $\text{Ge}_{16}\text{Cu}^-$ as $[1\text{S}^2 1\text{P}^6 1\text{D}^6 1\text{F}^6 1\text{D}^4 1\text{F}^8 3\text{d}_{\text{Cu}}^8 2\text{S}^2 2\text{P}^2 1\text{G}^6 2\text{P}^4 1\text{G}^{10} 2\text{D}^4 1\text{G}^2 2\text{D}^6]$. The images of the 3d_{Cu} orbitals are represented in the insert of Fig. 5.

3.3. Electron shell of 68 valence electrons and Jahn–Teller distortion

Let us now describe in some detail the electronic configurations of the neutral Ge_{16}Ti as well as the anionic $\text{Ge}_{16}\text{Sc}^-$ that possess

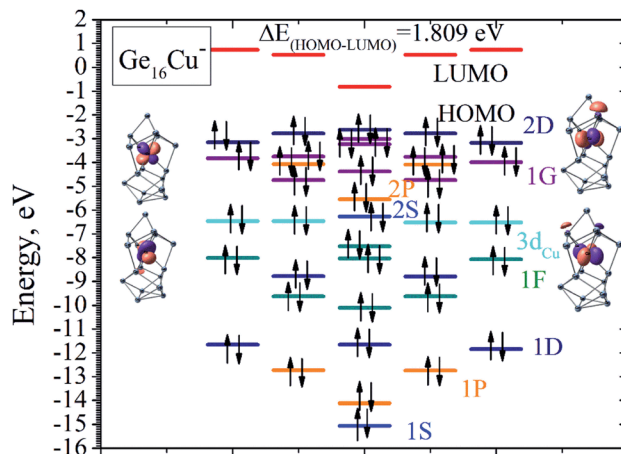


Fig. 5 A MO energy diagram of the $\text{Ge}_{16}\text{Cu}^-$ anionic cluster and the four 3d orbitals of the Cu dopant atom in the insert. Black arrow represents electron. Bright blue lines represent the 1S and 2S shell orbitals; orange for the 1P and 2P shell orbitals; dark blue for the 1D and 2D shell orbitals; green for the 1F shell orbitals; violet for the 1G shell orbitals; cyan lines for the 3d orbital of Cu and red lines represent HOMO of the cluster.

FK shape in T_d symmetry. Each Ge atom in Ge_{16}Ti contributes four valence electrons, whereas the Sc and Ti atom contribute three and four, respectively, to its cluster shell. The number of valence electrons contributed by the constitution atoms to the cluster shell amounts to 68 that occupy thus 34 shell MOs. As described in Section 3.2 above, the electronic configuration of this cluster can be written as $[1\text{S}^2 1\text{P}^6 1\text{D}^{10} 2\text{S}^2 1\text{F}^{14} 2\text{P}^6 1\text{G}^{18} 2\text{D}^{10}]$ in which the HOMO is the 2D shell and the LUMO is the 1H. In a T_d point group, the D shell orbitals of either Ge_{16}Ti or $\text{Ge}_{16}\text{Sc}^-$ split into 2-fold and 3-fold degenerate orbitals, corresponding to an E irreducible representation and a T irreducible representation, respectively, or it could be written as $D = E + T$. The F shell orbital of both Ge_{16}Ti and $\text{Ge}_{16}\text{Sc}^-$ split to 1-fold and 3-fold and 3-fold degenerate orbitals, namely $F = T + T + A$. In the same vein, the G shell orbital splits to 1-fold and 3-fold, 3-fold and 2-fold degeneracy orbitals, namely $G = A + 2T + E$. Therefore, the electron shell configuration of each cluster could be written as follows: $[1\text{S}^2 1\text{P}^6 1\text{D}_{2\text{-folds}}^4 1\text{D}_{3\text{-folds}}^6 2\text{S}^2 1\text{F}_{3\text{-folds}}^6 1\text{F}_{1\text{-fold}}^2 2\text{P}^6 1\text{G}_{1\text{-fold}}^2 1\text{G}_{3\text{-folds}}^6 1\text{G}_{3\text{-folds}}^6 1\text{G}_{2\text{-folds}}^4 2\text{D}^{10}]$.

A closer look at the shapes of shell MOs shows that the ordering of some shell MOs alters, and the shell electron configuration of the cluster becomes: $[1\text{S}^2 1\text{P}^6 1\text{D}_{2\text{-folds}}^4 1\text{D}_{3\text{-folds}}^6 1\text{F}_{1\text{-fold}}^2 1\text{F}_{3\text{-folds}}^6 1\text{F}_{3\text{-folds}}^6 2\text{S}^2 1\text{G}_{1\text{-fold}}^2 2\text{P}^6 1\text{G}_{3\text{-folds}}^6 1\text{G}_{3\text{-folds}}^6 1\text{G}_{2\text{-folds}}^4 2\text{D}_{2\text{-folds}}^4 2\text{D}_{3\text{-fold}}^6]$ as this can be seen in Fig. 6a and c.

Nevertheless, geometry optimizations reveal that only FK structures with a closed shell filled by 68 valence electrons, including neutral Ge_{16}Ti and anionic $\text{Ge}_{16}\text{Sc}^-$ clusters, possess a T_d high symmetry whereas the remaining FK structures, which enclose more or less than 68 valence electrons, exist at lower symmetry. Such a geometrical distortion can be understood by the Jahn–Teller effect. Let us first examine the open-shell neutral Ge_{16}Sc having 67 valence electrons due to the fact that the HOMO of the anion $\text{Ge}_{16}\text{Sc}^-$ is a 2D shell orbital; the latter



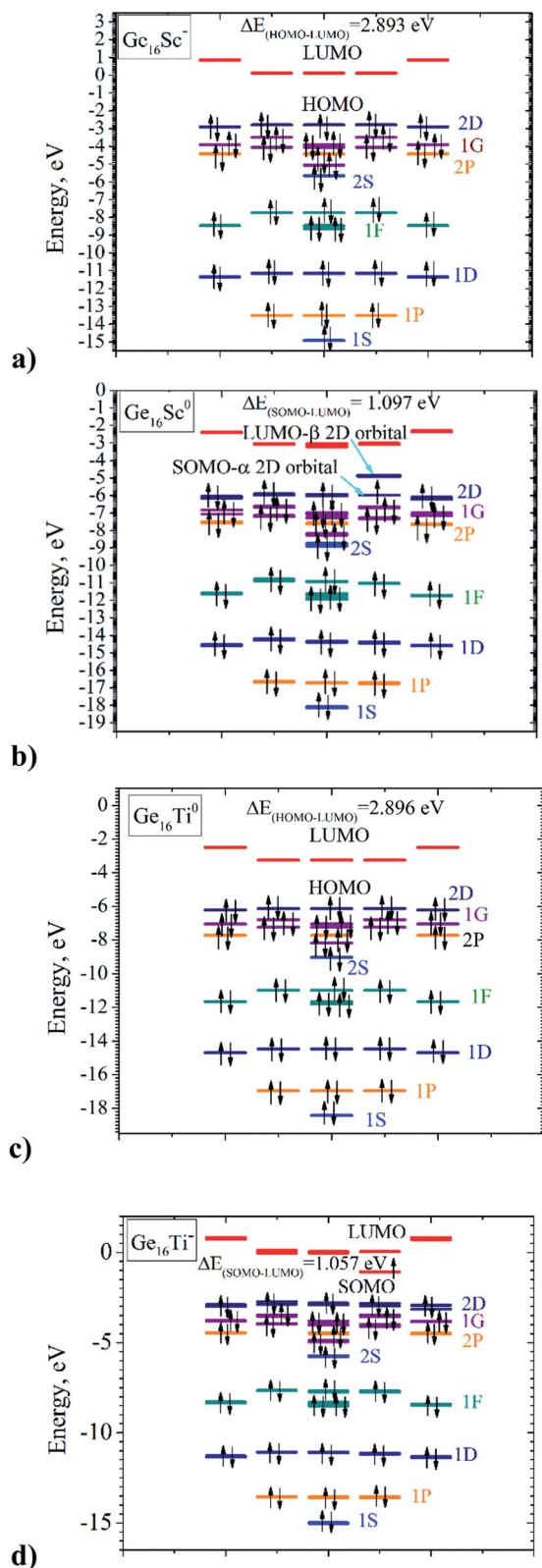


Fig. 6 MO diagrams of (a) $\text{Ge}_{16}\text{Sc}^-$ anion; (b) $\text{Ge}_{16}\text{Sc}^0$ neutral; (c) $\text{Ge}_{16}\text{Ti}^0$ neutral; and (d) $\text{Ge}_{16}\text{Ti}^-$ anion. Black arrow represents electron. Bright blue lines represent the 1S and 2S shell orbitals; orange for the 1P and 2P shell orbitals; dark blue for the 1D and 2D shell orbitals; green for the 1F shell orbitals; violet for the 1G shell orbitals, and red lines represent for HOMO of the clusters.

has the value of azimuthal quantum number l equal to 2 and a 5-fold degeneracy. In the T point group, the 2D shell orbitals are reduced to the E + T irreducible representations in which the T orbitals, or the $2\text{D}_{\text{three-fold}}$ levels are higher energetically. As an electron is removed from such a HOMO, namely the $2\text{D}_{\text{three-fold}}$ of the anionic $\text{Ge}_{16}\text{Sc}^-$, to form the neutral Ge_{16}Sc , the corresponding SOMO is triply degenerate and the T_d structure of the Ge_{16}Sc neutral is subjected to a distortion to a C_{3v} group, accompanying a splitting of the T MOs, or the $2\text{D}_{\text{three-fold}}$ one, into E + A_2 orbitals, and the A_2 orbital is now singly occupied (*cf.* Fig. 6b).

In the case of 69 electrons of the $\text{Ge}_{16}\text{Ti}^-$ anion, it is worth to note that the LUMO of the Ge_{16}Ti neutral cluster corresponds to a 1H shell orbital which has the value of azimuthal quantum number l of 5 and a 11-fold degeneracy. In the T point group, the 1H shell is reduced into E + 3T irreducible representations. In going from the neutral Ge_{16}Ti to the anionic $\text{Ge}_{16}\text{Ti}^-$, the incoming electron fills in one of the degenerate LUMO of T representation, which thus causes a distortion of the T_d structure of the Ge_{16}Ti neutral, again to a C_{3v} structure of the resulting $\text{Ge}_{16}\text{Ti}^-$ anion, accompanying with a splitting of the T MOs into E + A_2 orbitals, of which the A_2 orbital accommodates the unpaired electron (*cf.* Fig. 6d).

It is also worth mentioning that the vertical electron detachment energy between the neutral Ge_{16}Sc and its anion at the geometrical structure of the anion which has 68 electrons, amounts to 3.95 eV, whereas the adiabatic detachment energy is 3.81 eV. Thus, the energy gain of the Ge_{16}Sc neutral upon distortion is 0.14 eV. Similarly, the energy gain of $\text{Ge}_{16}\text{Ti}^-$ due to a distortion from T_d to C_{3v} symmetry is calculated at a value of 0.23 eV. Such a small but significant amount of energy originates in an intrinsic instability of the T^1 or the $2\text{D}_{\text{three-fold}}^1$ electron configuration of the HOMOs of Ge_{16}Sc , as well as the T^1 or $1\text{H}_{\text{three-fold}}^1$ configuration of the LUMOs of $\text{Ge}_{16}\text{Ti}^-$, all in T_d symmetry. The latter are therefore distorted to C_{3v} point group yielding such an energy gain of the system.

The SOMO–LUMO gap of 1.1 eV in the 67 electrons neutral Ge_{16}Sc is very close to the SOMO–LUMO gap in the 69 electrons of anionic $\text{Ge}_{16}\text{Ti}^-$. This reflects the fact that both systems undergo a comparable symmetry reduction when going from the $\text{Ge}_{16}\text{Sc}^-$ to Ge_{16}Sc as well as from Ge_{16}Ti to $\text{Ge}_{16}\text{Ti}^-$, as this is illustrated in Fig. 6b and d. In summary, two forces are combined in the formation of the C_{3v} structures of 67-electron Ge_{16}Sc neutral and 69 electron $\text{Ge}_{16}\text{Ti}^-$ anion: the major intrinsic stability of the 68 electron $\text{Ge}_{16}\text{Sc}^-$ and Ge_{16}Ti counterparts which favor a T_d symmetry, and the reorganization energy gained during the symmetry lowering from T_d to C_{3v} point group. This also makes the average binding energy of $\text{Ge}_{16}\text{Sc}^-$ much higher than that of its neutral, while the average binding energy of $\text{Ge}_{16}\text{Ti}^-$ is only slightly higher.

3.4. Spin magnetic moments

It is typical that when a metallic cluster is doped by a transition metal atom, the outer-most orbitals of the impurity including d and s shell can combine with the valence orbitals of the host to form shell orbitals of the resulting doped clusters. For the



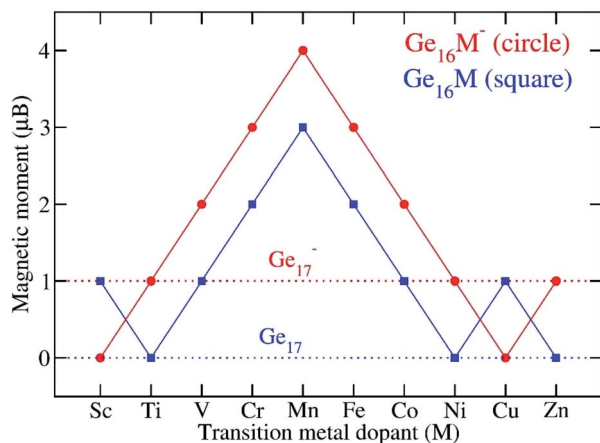


Fig. 7 Total spin magnetic moment (μ_B) of Ge_{16}M in comparison with Ge_{17} at both neutral and anionic states.

investigated Ge_{16}M , as each Ge atom delocalizes its 4 valence electrons, the corresponding Ge_{16}M^- anion can approach 68 electrons if the metal dopant could delocalize its 3 valence electrons. The remaining valence electrons of the metal will combine to build up its magnetic moment. Fig. 7 shows the change in the total spin magnetic moment (TMM) value of Ge_{16}M in both neutral and anionic states as M goes from Sc to Zn. The perception of how the total and local spin magnetic moments of the clusters arise can be confirmed in considering the calculated total and local spin magnetic moments on each constituent atoms of the clusters that are listed in Table 1. The total spin magnetic moment of the Ge_{16}M^- anion increases steadily from 1 μ_B for the Ti dopant to 4 μ_B for the Mn dopant, then decreases to 1 μ_B for the Ni dopant. For the Ge_{16}M^- anions, their magnetic moments are mostly held on the transition metal atoms, being 0.4, 1.5, 2.9, 3.1, 2.2, and 1.4 for the Ti, V, Cr, Mn, Fe, and Co dopants, respectively. Exceptions include the $\text{Ge}_{16}\text{Ni}^-$ and $\text{Ge}_{16}\text{Zn}^-$ in which the total magnetic moments are delocalized all over the entire skeleton.

In order to gain more insight into the spin magnetic behavior of Ge_{16}M clusters, along with Table 1 listing total and local spin magnetic moments, the total density of states (TDOS) and partial density of states (PDOS) of the anionic Ge_{16}M^- clusters from the Ti to Ni dopants are plotted in Fig. 8. Spin-up and spin-down densities of states are plotted separately on the same graph for each of the clusters. It has been stated that the relative shift between the spin-up and spin-down bands indicates the degree of spin-exchange splitting; the larger the shift of DOS bands, the larger the magnetic moment of the cluster.⁵⁵ As we glance at Fig. 8, we can realize that the shift is large for the Ge_{16}M^- ($\text{M} = \text{Cr}, \text{Mn}, \text{Fe}, \text{Co}$) clusters suggesting that they possess high spin magnetic moments, while it is slight in the cases of $\text{Ge}_{16}\text{Ti}^-$ and $\text{Ge}_{16}\text{Ni}^-$ clusters.

The spin magnetic moment of the whole cluster is mainly created by the unpaired electrons, and the spin magnetic moments localized on the metal dopant arise from the density of unpaired electron contained in its orbitals or the difference in partial density of α - and β -electrons of the M atom. For the Ti

and V clusters (Fig. 8a and b), the α -HOMO states are located at distinctive energy level as compared to the α -, β -inner states, while for the other Ge_{16}M , with M being Cr, Mn, Fe, Co, and Ni, the α -HOMO states are situated in almost the same energy region as with the α -, and β -inner states. For the DOS of $\text{Ge}_{16}\text{Cr}^-$ anion, in the domain of states ranging from -4.3 to -2.0 eV, there is an obvious presence of the density of α -state of d orbitals of Cr (the blue curve) without the β -state counterpart. This information implies that the total magnetic moment of the cluster is mainly dominated by Cr-d states, while Ge-s and Ge-p states make rather a small contribution. A similar argument can be made for the successive clusters. For $\text{Ge}_{16}\text{Mn}^-$ in the domain from *ca.* -6.5 to -2.0 eV there are densities of α -states of s- and d-orbitals of Mn (the green and blue curves) without their β -state counterparts; for $\text{Ge}_{16}\text{Fe}^-$ in the domain from *ca.* -7.0 to -2.0 eV there are densities of α -states of s- and d-orbitals of Fe (the green and blue curves) without their β -state counterparts; for $\text{Ge}_{16}\text{Co}^-$ in the domain from *ca.* -7.0 to -2.0 eV there are densities of α -states of s- and d-orbitals of Co (the green and blue curves) without their β -state counterparts. This observation is in line with the calculated local magnetic moments on the Cr, Mn, Fe, Co atoms which amount to 2.9, 3.1, 2.2 and 1.4 μ_B , respectively. Thus, although the Ge_{16} cage somehow quenches the usually large magnetic moments of free transition metal atoms, the latter property remain substantial in the doped derivatives.

3.5. IR spectra

As discussed above, several lower-energy structural and spin isomers for each Ge_{16}M cluster are considered, and we report herein only the lowest-energy isomers for certain species. In some cases, the energy difference of the most stable isomers is really small that cannot allow us to distinguish the ground state structure. Moreover, no infrared (IR) spectrum of any Ge_nM has been reported both experimentally and theoretically so far. The IR spectra are expected to provide us with a fingerprint for assignment of the cluster in terms of their metallic dopant, especially for the geometrical structure. For the purpose to help for distinguishing low-lying energy isomers, the calculated vibrational spectra of two lowest-lying isomers for some selected Ge_{16}M , namely the Ge_{16}Sc and Ge_{16}Ti in both neutral and anionic forms, are plotted in Fig. 9. The vibrational frequency range goes from 0 to 350 cm^{-1} , as no signals are found at higher photon energy. As it could be seen in Fig. 9a and b, the vibrational spectra for the ground state of $\text{Ge}_{16}\text{Sc}^-$ anion and Ge_{16}Ti neutral, each has 68 valence electrons and is in T_d symmetry, are relatively simple featuring a highly intense peak, centered at ~ 304 and 292 cm^{-1} with T degenerate modes, respectively.

Unlike the IR spectra of the ground states, those of the next isomers turn out to be more complicated and characterized by several highly intense peaks in the range of 260 to 300 cm^{-1} (see Fig. 9c and d). The following frequencies can be noted. While for the ground state of Ge_{16}Sc neutral, isomer **n.Sc.A** has $\nu_{\text{stretching Sc-Ge}}$ being of ~ 298 cm^{-1} , the $\nu_{\text{stretching Sc-Ge}}$ of the next isomer **n.Sc.B** is of ~ 280 and 290 cm^{-1} . For the $\text{Ge}_{16}\text{Sc}^-$ anion,



Table 1 Total spin magnetic moment (TMM, μ_B) of Ge_{16}M and local spin magnetic moment (LMM, μ_B) of each atom at (a) neutral and (b) anionic states. Atom number and corresponding Cartesian coordinates of each atom in Ge_{16}M are given in the Table S1 of the ESI

| (a) | | | | | | | | | |
|---------|----------------------------------|---------------------------------|----------------------------------|----------------------------------|----------------------------------|----------------------------------|----------------------------------|----------------------------------|-------------------------------|
| Atom | Ge ₁₆ Sc | Ge ₁₆ V | Ge ₁₆ Cr | Ge ₁₆ Mn | Ge ₁₆ Fe | Ge ₁₆ Co [−] | Ge ₁₆ Cu | | |
| Ge (1) | 0.0 | 0.1 | −0.3 | 0.0 | 0.1 | 0.0 | 0.0 | | |
| Ge (2) | 0.0 | 0.0 | 0.0 | 0.0 | 0.0 | 0.0 | 0.0 | | |
| Ge (3) | 0.1 | 0.0 | 0.0 | 0.0 | 0.0 | 0.0 | 0.1 | | |
| Ge (4) | 0.1 | −0.1 | 0.0 | 0.0 | 0.0 | 0.0 | 0.1 | | |
| Ge (5) | 0.1 | 0.0 | −0.1 | 0.0 | 0.1 | 0.0 | 0.0 | | |
| Ge (6) | 0.0 | 0.0 | 0.0 | 0.0 | 0.0 | 0.0 | 0.0 | | |
| Ge (7) | 0.0 | 0.0 | 0.0 | 0.0 | 0.0 | 0.0 | 0.1 | | |
| Ge (8) | 0.0 | 0.0 | 0.0 | 0.0 | 0.0 | 0.0 | 0.1 | | |
| Ge (9) | 0.0 | 0.0 | 0.0 | 0.0 | 0.0 | 0.0 | 0.0 | | |
| Ge (10) | 0.3 | 0.1 | 0.0 | 0.0 | 0.0 | 0.0 | 0.0 | | |
| Ge (11) | 0.0 | −0.1 | −0.1 | 0.0 | 0.1 | 0.0 | 0.0 | | |
| Ge (12) | 0.0 | 0.0 | −0.1 | 0.1 | 0.1 | 0.0 | 0.4 | | |
| Ge (13) | 0.1 | 0.1 | 0.0 | 0.1 | 0.1 | 0.1 | 0.1 | | |
| Ge (14) | 0.0 | 0.0 | 0.0 | 0.0 | 0.0 | 0.0 | 0.1 | | |
| Ge (15) | 0.0 | 0.0 | 0.0 | 0.1 | −0.1 | 0.0 | 0.0 | | |
| Ge (16) | 0.1 | −0.1 | 0.0 | 0.0 | −0.1 | 0.0 | 0.0 | | |
| M (17) | 0.2 | 1.0 | 2.6 | 2.7 | 1.7 | 0.9 | 0.0 | | |
| TMM | 1.0 | 1.0 | 2.0 | 3.0 | 2.0 | 1.0 | 1.0 | | |
| (b) | | | | | | | | | |
| Atom | Ge ₁₆ Ti [−] | Ge ₁₆ V [−] | Ge ₁₆ Cr [−] | Ge ₁₆ Mn [−] | Ge ₁₆ Fe [−] | Ge ₁₆ Co [−] | Ge ₁₆ Ni [−] | Ge ₁₆ Zn [−] | Ge ₁₇ [−] |
| Ge (1) | 0.1 | −0.1 | 0.0 | 0.1 | 0.1 | 0.1 | 0.0 | 0.0 | 0.0 |
| Ge (2) | 0.0 | 0.0 | 0.1 | 0.0 | 0.1 | 0.0 | 0.0 | 0.1 | 0.1 |
| Ge (3) | 0.0 | 0.1 | 0.1 | 0.0 | 0.0 | 0.0 | 0.2 | 0.1 | 0.0 |
| Ge (4) | 0.0 | 0.0 | 0.1 | 0.0 | 0.0 | 0.0 | 0.0 | 0.1 | 0.0 |
| Ge (5) | 0.0 | 0.0 | 0.0 | 0.1 | 0.1 | 0.0 | 0.1 | 0.0 | 0.0 |
| Ge (6) | 0.0 | 0.0 | 0.0 | 0.1 | 0.1 | 0.1 | 0.1 | 0.0 | 0.0 |
| Ge (7) | 0.0 | 0.0 | 0.0 | 0.0 | 0.0 | 0.0 | 0.0 | 0.1 | 0.0 |
| Ge (8) | 0.1 | 0.1 | 0.0 | 0.0 | 0.0 | 0.0 | 0.1 | 0.1 | 0.1 |
| Ge (9) | 0.1 | 0.0 | 0.0 | 0.0 | 0.0 | 0.1 | 0.1 | 0.0 | 0.0 |
| Ge (10) | 0.0 | 0.0 | 0.0 | 0.1 | 0.1 | 0.1 | 0.0 | 0.0 | 0.1 |
| Ge (11) | 0.0 | 0.1 | 0.0 | 0.1 | 0.0 | 0.0 | 0.0 | 0.1 | 0.1 |
| Ge (12) | 0.1 | 0.0 | 0.0 | 0.2 | 0.2 | 0.2 | 0.0 | 0.1 | 0.1 |
| Ge (13) | 0.1 | 0.1 | −0.1 | 0.0 | 0.0 | 0.0 | 0.1 | 0.1 | 0.0 |
| Ge (14) | 0.0 | 0.1 | −0.1 | 0.0 | 0.0 | 0.0 | 0.1 | 0.1 | 0.5 |
| Ge (15) | 0.1 | 0.0 | −0.1 | 0.1 | 0.1 | 0.0 | 0.0 | 0.1 | 0.0 |
| Ge (16) | 0.0 | 0.1 | 0.1 | 0.1 | 0.0 | 0.0 | 0.0 | 0.0 | 0.0 |
| M (17) | 0.4 | 1.5 | 2.9 | 3.1 | 2.2 | 1.4 | 0.2 | 0.0 | 0.0 |
| TMM | 1.0 | 2.0 | 3.0 | 4.0 | 3.0 | 2.0 | 1.0 | 1.0 | 1.0 |

FK structure **a.Sc.A** has a $\nu_{\text{stretching Sc-Ge}}$ of $\sim 304 \text{ cm}^{-1}$, while $\nu_{\text{stretching Sc-Ge}}$ of the isomer **a.Sc.B** is of $\sim 264, 279$ and 289 cm^{-1} . Although for Ge_{16}Ti , FK structure **n.Ti.A** only has one peak at 292 cm^{-1} , being three-fold degenerate Sc-Ge stretching mode, for the next isomer **n.Ti.B**, the Sc-Ge stretching modes appear at three frequencies $\sim 263, 275$ and 298 cm^{-1} . For the anion $\text{Ge}_{16}\text{Ti}^-$, **a.Ti.A** in distorted FK shape (C_{3v}) leads its $\nu_{\text{stretching Sc-Ge}}$ being of ~ 246 and 281 cm^{-1} , which is a two-fold degenerate mode E, while **a.Ti.B** isomer has a $\nu_{\text{stretching Sc-Ge}}$ being of $\sim 252, 270$ and 279 cm^{-1} . The large difference in vibrational spectra for both nearly degenerate isomers and their high intense peaks can be used to assign the ground state structure when they can be generated experimentally and characterized spectroscopically.

By analysis of their IR spectra, a symmetry lowering of the cluster in going down from 68 to 67 as well as going up to 69 valence electrons can be recognized. The IR spectrum of Ge_{16}Ti is characterized by a single peak centered at 292 cm^{-1} , corresponding to the vibrational modes of Ti atom inside the Ge_{16} cage. Although the cluster has 45 vibrational modes in total, only the vibrational modes of the Ti atom inside the cage are IR active with notably high intensity. Other modes that correspond to deformation of the Ge_{16} cage do not result in significant IR intensity. The stretching modes of the Ti atom inside the Ge_{16} cage belong to the T_2 irreducible representation. As the cluster receives one electron to form the $\text{Ge}_{16}\text{Ti}^-$, the anion is distorted to C_{3v} point group and the $\nu(\text{Ti-Ge}_{16})$ T_2 mode is reduced to the $E + A_2$ modes. As this could be seen in Fig. 9, the difference of



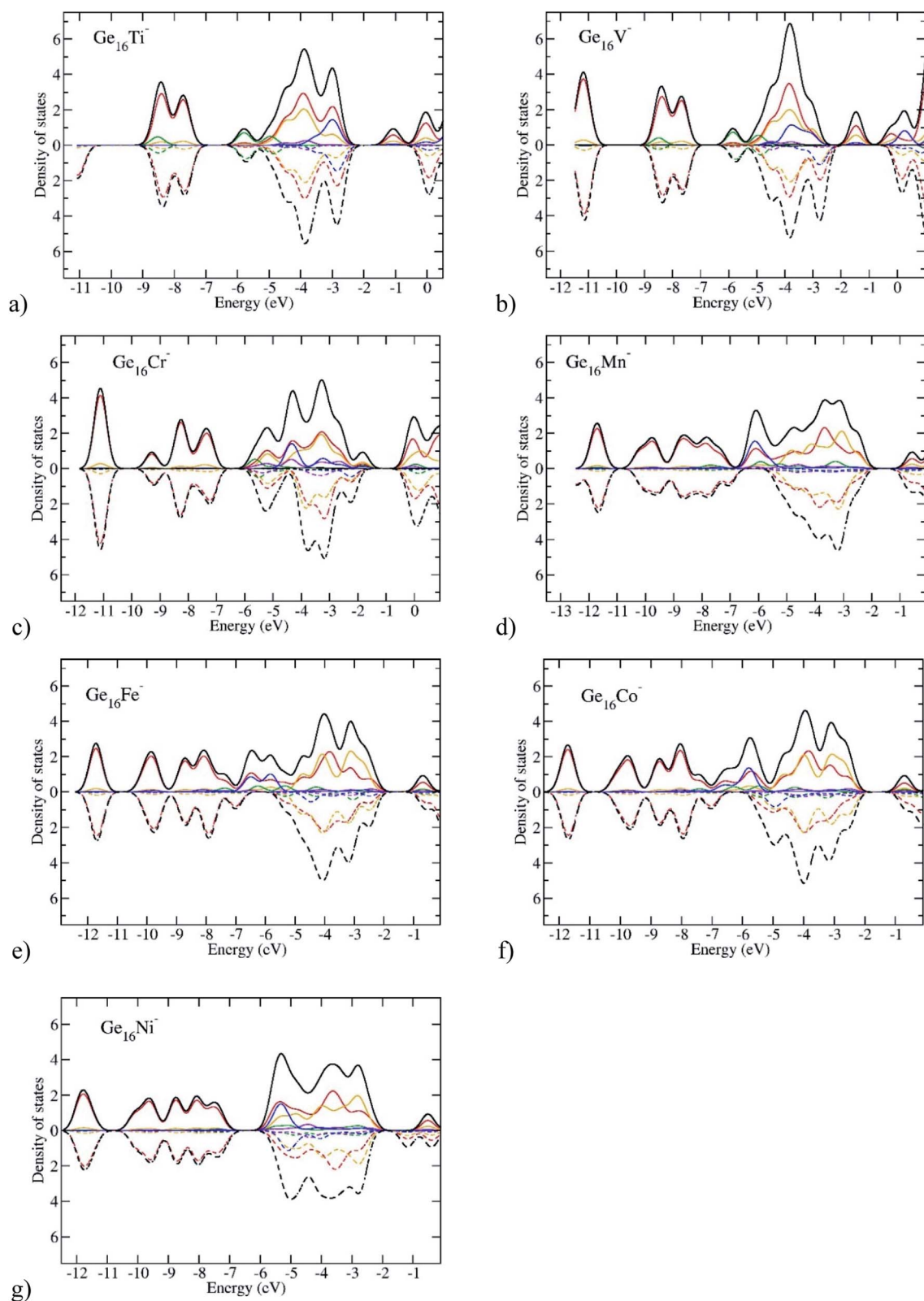


Fig. 8 Plots of density of states of $\text{Ge}_{16}\text{TM}^-$ anionic clusters. The red lines represent for the s states of Ge, the orange for the p states of Ge, the green for the s state of TM, the violet for the p states of TM, the blue for the d states of TM and the black lines represent for the total density of states. Solid lines represent for alpha spin states, and dashed lines for beta spin states.

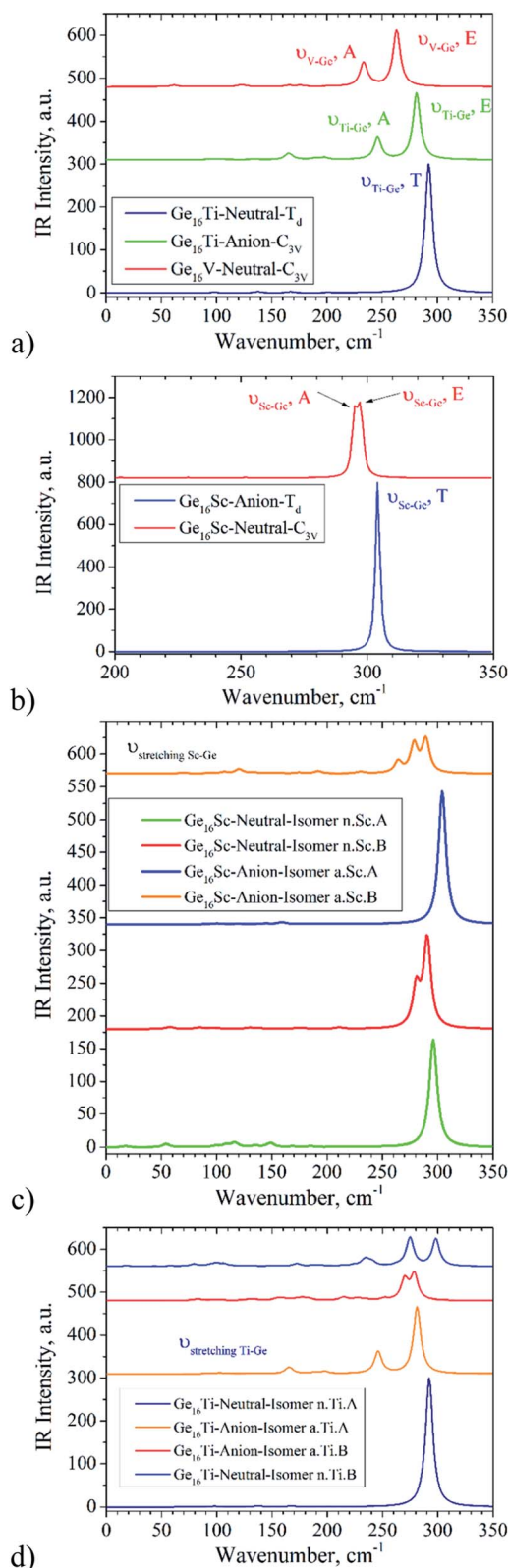


Fig. 9 The IR spectra of: (a) $\text{Ge}_{16}\text{Ti}^{0/-}$ and Ge_{16}V . The red curve represents for IR spectrum of Ge_{16}V neutral, the green curve for $\text{Ge}_{16}\text{Ti}^-$ anion, and the dark blue for the Ge_{16}Ti neutral; (b) $\text{Ge}_{16}\text{Sc}^{0/-}$ clusters. The red curve represents for the Ge_{16}Sc neutral, and the blue for the $\text{Ge}_{16}\text{Sc}^-$ anion; (c) the two lowest-energy isomers of the $\text{Ge}_{16}\text{Sc}^{0/-}$; (d) the two lowest-energy isomers of the $\text{Ge}_{16}\text{Ti}^{0/-}$.

22 cm^{-1} between the E and A_2 modes is relatively significant in view of the low frequency. It is worth noting that for $\text{Ge}_{16}\text{Ti}^-$, its $A_2 \nu(\text{Ti-Ge}_{16})$ stretching mode has a lower frequency than the E $\nu(\text{Ti-Ge}_{16})$ stretching. The added electron in the $\text{Ge}_{16}\text{Ti}^-$ anion causes the cluster to distort from T_d to C_{3v} point group, giving rise to a lowering of electron density along one of the three $\nu(\text{Ti-Ge}_{16})$ stretching modes.

4. Concluding remarks

In the present theoretical study, the geometric and electronic structures, thermodynamic stability, and magnetic properties of the 16-atom germanium clusters doped with the first-row 3d transition metal atoms, Ge_{16}M with $\text{M} = \text{Sc}, \text{Ti}, \text{V}, \text{Cr}, \text{Mn}, \text{Fe}, \text{Co}, \text{Ni}, \text{Cu},$ and Zn , in both neutral and anionic states, were investigated using quantum chemical (DFT) methods.

The most stable isomers of Ge_{16}M , as M goes from Sc to V, prefer a Frank-Kasper (FK) structure in which the metal dopant is endohedrally encapsulated at the central position of a Ge_{16} FK cage. In particular, both the anionic $\text{Ge}_{16}\text{Sc}^-$ and neutral Ge_{16}Ti whose electronic shells are filled by a magic number of 68 valence electrons, are characterized by a perfect FK tetrahedral geometry and enjoy an enhanced thermochemical stability with high average binding energies and embedding energies. Their higher stability can be interpreted in terms of the electronic shells of the Jellium model. Analyses of electronic configuration also indicate that the geometric distortions from an FK tetrahedron Ge_{16}M having more or less than 68 valence electrons are caused by a Jahn-Teller effect arising from the degenerate frontier orbitals.

Perhaps most interestingly is the result obtained from energy calculations that revealed that both neutrals Ge_{16}Sc and Ge_{16}Cu emerge as superhalogens, due to a characteristic that each possesses a large electron affinity of 3.8 and 3.6 eV, respectively. These electron affinities exceed the values of halogen atoms and even that of the well-known superhalogen Al_{13} (~ 3.6 eV). Moreover, a comprehensive picture of the magnetic behavior is displayed for Ge_{16}M clusters at both neutral and anionic states, in which the observed dopant-dependent magnetic moment can be understood by a charge distribution analysis. As M goes from the left to the right side on the first-row transition metal atoms in the Periodic Table, corresponding to Sc to Zn, the total magnetic moment of Ge_{16}M first takes a low value at $\text{M} = \text{Sc}$ and Ti, then increases steadily and reaches the maximum value of $3\mu_B$ at $\text{M} = \text{Mn}$, before decreasing towards the end of the row due to the fact that these magnetic moments are mostly held on the metal dopants. This result opens up an avenue that a magnetically inert germanium cluster can be induced to a relatively high magnetic moment following doping by a suitable transition metal impurity. Finally, the IR spectra of FK Ge_{16}M are simulated as a helpful guide for future experimental assignment of these degenerate ground state clusters.

Funding information

This work is funded by VinGroup (Vietnam) and supported by VinGroup Innovation Foundation (VinIF) under project code VinIF.2020.DA21.



Conflicts of interest

There are no conflicts of interest to declare.

References

- 1 E. F. Archibong and A. St-Amant, *J. Chem. Phys.*, 1998, **109**, 962–972.
- 2 K. A. Gingerich, R. W. Schmude, M. Sai Baba and G. Meloni, *J. Chem. Phys.*, 2000, **112**, 7443–7448.
- 3 B.-x. Li and P.-l. Cao, *Phys. Rev. B: Condens. Matter Mater. Phys.*, 2000, **62**, 15788–15796.
- 4 Z.-Y. Lu, C.-Z. Wang and K.-M. Ho, *Phys. Rev. B: Condens. Matter Mater. Phys.*, 2000, **61**, 2329–2334.
- 5 J. Zhao, J. Wang and G. Wang, *Phys. Lett. A*, 2000, **275**, 281–286.
- 6 C. Zhao and K. Balasubramanian, *J. Chem. Phys.*, 2001, **115**, 3121–3133.
- 7 S. Ma and G. Wang, *J. Mol. Struct.: THEOCHEM*, 2006, **767**, 75–79.
- 8 G. Pacchioni and J. Koutecký, *J. Chem. Phys.*, 1986, **84**, 3301–3310.
- 9 J. Wang, G. Wang and J. Zhao, *Phys. Rev. B: Condens. Matter Mater. Phys.*, 2001, **64**, 205411.
- 10 S. Bulusu, S. Yoo and X. C. Zeng, *J. Chem. Phys.*, 2005, **122**, 164305.
- 11 W. An, *Phys. Chem. Chem. Phys.*, 2018, **20**, 25746–25751.
- 12 S. M. Beck, *J. Chem. Phys.*, 1987, **87**, 4233–4234.
- 13 V. Kumar and Y. Kawazoe, *Phys. Rev. B: Condens. Matter Mater. Phys.*, 2002, **65**, 073404.
- 14 J. Zhao, Q. Du, S. Zhou and V. Kumar, *Chem. Rev.*, 2020, **120**, 9021–9163.
- 15 J. De Haeck, T. B. Tai, S. Bhattacharyya, H. T. Le, E. Janssens, M. T. Nguyen and P. Lievens, *Phys. Chem. Chem. Phys.*, 2013, **15**, 5151–5162.
- 16 G. Gopakumar, P. Lievens and M. T. Nguyen, *J. Phys. Chem. A*, 2007, **111**, 4353–4361.
- 17 V. T. Ngan, J. De Haeck, H. T. Le, G. Gopakumar, P. Lievens and M. T. Nguyen, *J. Phys. Chem. A*, 2009, **113**, 9080–9091.
- 18 N. M. Tam, V. T. Ngan and M. T. Nguyen, *Chem. Phys. Lett.*, 2014, **595–596**, 272–276.
- 19 X.-J. Li and K.-H. Su, *Theor. Chem. Acc.*, 2009, **124**, 345.
- 20 S. Mahtout, C. Siouani and F. Rabilloud, *J. Phys. Chem. A*, 2018, **122**, 662–677.
- 21 S. Shi, Y. Liu, C. Zhang, B. Deng and G. Jiang, *Comput. Theor. Chem.*, 2015, **1054**, 8–15.
- 22 K. Dhaka, R. Trivedi and D. Bandyopadhyay, *J. Mol. Model.*, 2013, **19**, 1473–1488.
- 23 X.-J. Hou, G. Gopakumar, P. Lievens and M. T. Nguyen, *J. Phys. Chem. A*, 2007, **111**, 13544–13553.
- 24 Y. Jin, S. Lu, A. Hermann, X. Kuang, C. Zhang, C. Lu, H. Xu and W. Zheng, *Sci. Rep.*, 2016, **6**, 30116.
- 25 M. Kumar, N. Bhattacharyya and D. Bandyopadhyay, *J. Mol. Model.*, 2012, **18**, 405–418.
- 26 X.-Q. Liang, X.-J. Deng, S.-J. Lu, X.-M. Huang, J.-J. Zhao, H.-G. Xu, W.-J. Zheng and X. C. Zeng, *J. Phys. Chem. C*, 2017, **121**, 7037–7046.
- 27 C. Liu, I. A. Popov, L.-J. Li, N. Li, A. I. Boldyrev and Z.-M. Sun, *Chem.–Eur. J.*, 2018, **24**, 699–705.
- 28 W. Qin, W.-C. Lu, L.-H. Xia, L.-Z. Zhao, Q.-J. Zang, C. Z. Wang and K. M. Ho, *AIP Adv.*, 2015, **5**, 067159.
- 29 C. Siouani, S. Mahtout, S. Safer and F. Rabilloud, *J. Phys. Chem. A*, 2017, **121**, 3540–3554.
- 30 V. T. Tran, M. T. Nguyen and Q. T. Tran, *J. Phys. Chem. A*, 2017, **121**, 7787–7796.
- 31 V. T. Tran and Q. T. Tran, *J. Comput. Chem.*, 2018, **39**, 2103–2109.
- 32 R. Trivedi, K. Dhaka and D. Bandyopadhyay, *RSC Adv.*, 2014, **4**, 64825–64834.
- 33 J. Wang and J.-G. Han, *J. Phys. Chem. A*, 2006, **110**, 12670–12677.
- 34 V. Kumar and Y. Kawazoe, *Appl. Phys. Lett.*, 2003, **83**, 2677–2679.
- 35 D. Bandyopadhyay, P. Kaur and P. Sen, *J. Phys. Chem. A*, 2010, **114**, 12986–12991.
- 36 J. Atobe, K. Koyasu, S. Furuse and A. Nakajima, *Phys. Chem. Chem. Phys.*, 2012, **14**, 9403–9410.
- 37 S. Jaiswal and V. Kumar, *Comput. Theor. Chem.*, 2016, **1075**, 87–97.
- 38 H. T. Pham, C.-T. D. Phan, M. T. Nguyen and N. M. Tam, *RSC Adv.*, 2020, **10**, 19781–19789.
- 39 N. A. Borshch, N. S. Pereslavl'tseva and S. I. Kurganskii, *Russ. J. Phys. Chem. B*, 2015, **9**, 9–18.
- 40 V. Kumar and Y. Kawazoe, *Phys. Rev. Lett.*, 2001, **87**, 045503.
- 41 V. Kumar and Y. Kawazoe, *Phys. Rev. Lett.*, 2002, **88**, 235504.
- 42 V. Kumar and Y. Kawazoe, *Appl. Phys. Lett.*, 2002, **80**, 859–861.
- 43 V. Kumar, A. K. Singh and Y. Kawazoe, *Nano Lett.*, 2004, **4**, 677–681.
- 44 A. K. Singh, V. Kumar and Y. Kawazoe, *J. Phys. Chem. B*, 2005, **109**, 15187–15189.
- 45 Q. Du, Z. Wang, S. Zhou, J. Zhao and V. Kumar, *Phys. Rev. Mater.*, 2021, **5**, 066001.
- 46 N. D. Minh, C. H. Cuong, N. T. Trung and V. T. Ngan, *Theor. Chem. Acc.*, 2018, **137**, 131.
- 47 M. J. Frisch, H. B. Schlegel, G. E. Scuseria, M. A. Robb, J. R. Cheeseman, J. A. Montgomery, *et al.*, *Gaussian 09 Revision: D.01*, 2009.
- 48 T. B. Tai and M. T. Nguyen, *J. Chem. Theory Comput.*, 2011, **7**, 1119–1130.
- 49 M. Saunders, *J. Comput. Chem.*, 2004, **25**, 621–626.
- 50 E. Bergeron Denis, A. W. Castleman, T. Morisato and N. Khanna Shiv, *Science*, 2004, **304**, 84–87.
- 51 Q. A. Smith and M. S. Gordon, *J. Phys. Chem. A*, 2011, **115**, 899–903.
- 52 M. Brack, *Rev. Mod. Phys.*, 1993, **65**, 677–732.
- 53 N. M. Tam, T. B. Tai and M. T. Nguyen, *J. Phys. Chem. C*, 2012, **116**, 20086–20098.
- 54 N. M. Tam, T. B. Tai, V. T. Ngan and M. T. Nguyen, *J. Phys. Chem. A*, 2013, **117**, 6867–6882.
- 55 C.-G. Li, J. Zhang, W.-Q. Zhang, Y.-N. Tang, B.-Z. Ren and Y.-F. Hu, *Sci. Rep.*, 2017, **7**, 17516.

